Electrodeless plasma acceleration system using rotating magnetic field method

T. Furukawa, K. Takizawa, D. Kuwahara, and S. Shinohara
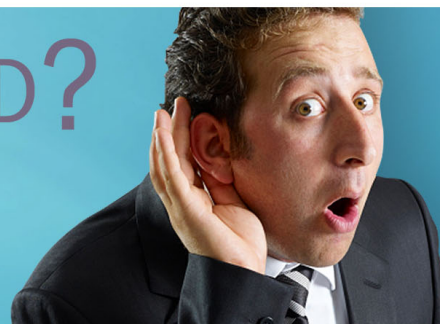
Electrodeless plasma acceleration system using rotating magnetic field method

T. Furukawa,[1,a] K. Takizawa,[1] D. Kuwahara,[2] and S. Shinohara[2]
[1]*The Graduate School of Engineering, Tokyo University of Agriculture and Technology, Tokyo 184-8588, Japan*
[2]*Institute of Engineering, Tokyo University of Agriculture and Technology, Tokyo 184-8588, Japan*

We have proposed Rotating Magnetic Field (RMF) acceleration method as one of electrodeless plasma accelerations. In our experimental scheme, plasma generated by an rf (radio frequency) antenna, is accelerated by RMF antennas, which consist of two-pair, opposed, facing coils, and these antennas are outside of a discharge tube. Therefore, there is no wear of electrodes, degrading the propulsion performance. Here, we will introduce our RMF acceleration system developed, including the experimental device, e.g., external antennas, a tapered quartz tube, a vacuum chamber, external magnets, and a pumping system. In addition, we can change RMF operation parameters (RMF applied current I_{RMF} and RMF current phase difference ϕ, focusing on RMF current frequency f_{RMF}) by adjusting matching conditions of RMF, and investigate the dependencies on plasma parameters (electron density n_{e} and ion velocity v_{i}); e.g., higher increases of n_{e} and v_{i} (~360 % and 55 %, respectively) than previous experimental results were obtained by decreasing f_{RMF} from 5 MHz to 0.7 MHz, whose RMF penetration condition was better according to Milroy's expression. Moreover, time-varying component of RMF has been measured directly to survey the penetration condition experimentally. © *2017 Author(s). All article content, except where otherwise noted, is licensed under a Creative Commons Attribution (CC BY) license (http://creativecommons.org/licenses/by/4.0/).* https://doi.org/10.1063/1.4998248

I. INTRODUCTION

In the field of a space propulsion, electric propulsion systems have been studied due to an advantage of the higher fuel efficiency than that of chemical ones. However, conventional electric thrusters, e.g., gridded ion thruster,[1] Hall thruster,[2] and Magneto-Plasma-Dynamics (MPD) thruster,[3] have electrodes, which contact with plasma directly, and this interaction makes an operating time limited and a long space exploration difficult because of the erosion of the electrodes.

In order to accomplish a longer operating time, which is in proportion to a specific impulse (exhaust velocity divided by gravitational acceleration), and high thrust performance for a next generation space propulsion scheme, some electrodeless plasma thrusters have been proposed and studied on, e.g., Electron Cyclotron Resonance (ECR) plasma thruster,[4] Variable Specific Impulse Magneto-plasma Rocket (VASIMR),[5] ratio frequency (rf) plasma thruster.[6] In these acceleration schemes, the plasma production and heating are conducted by external rf antennas, employing microwave ECR, Ion Cyclotron Heating (ICH), and a magnetic expansion scheme (so-called a magnetic nozzle). Among all, helicon electrodeless plasma acceleration,[6–8] using a helicon wave[9] excitation to generate plasmas (electron density n_{e} is up to ~ 10^{13} cm^{-3}) with additional acceleration methods have been studied under the Helicon Electrodeless Advanced Thruster (HEAT)[7,8] project.

Here, we have proposed one of the electrodeless plasma accelerations, i.e., Rotating Magnetic Field (RMF)[10,11] acceleration scheme.[7,8,12,13] This RMF method comes from the field of magnetically

---

[a]Electronic mail: s172832r@st.go.tuat.ac.jp

confined plasma fusion research in order to induce an azimuthal current to maintain the Field Reversed Configuration (RFC). In this acceleration scheme, an rf antenna, which is outside of a discharge tube, is used to produce a plasma, and the plasma acceleration is conducted by two pairs of opposed, facing RMF coils, wound around the discharge tube in the downstream of the plasma generation region. In our acceleration stage, the RMF coils are expected to induce an azimuthal current j_θ, whose mechanism will be shown in the next section, and plasmas can be accelerated by the axial Lorentz force f_z by the product of induced j_θ and a radial component of an applied external magnetic field B_r. Here, the process of generating f_z is described in Sec. II. It is very novel to apply this method to electromagnetic plasma acceleration under the divergent magnetic field, and this method will be a next generation electric propulsion scheme, if promising.

Our RMF experiment has been conducted using the Large Mirror Device (LMD),[14] and we can install RMF system and diagnostic instruments, which will be described in Sec. III. In our previous study on RMF acceleration, we applied RMF with RMF current frequency f_{RMF} = 5 MHz,[12] and surveyed the operation parameters (rf power P_{rf}, gas flow rate fr, and external magnetic field).[15] Here, we found that RMF could penetrate fully at a radial position of discharge tube r = 60 mm, where plasma radius R is 85 mm, and partially at r = 0 ∼ 45 mm into plasma, respectively, according to the Milroy's expression of RMF penetration condition.[11] Recently, dependences of an electron density n_e and ion velocity v_i on f_{RMF} have been investigated by changing f_{RMF} form 5 MHz to 3 MHz.[13] Higher increasing rates of n_e and v_i denoted as $\Delta n_e/n_e$ and $\Delta v_i/v_i$, respectively, have been obtained: up to ∼ 70 % and 28 %, respectively with f_{RMF} = 3 MHz than these with 5 MHz.[10] We have also examined the RMF operation conditions, e.g., RMF current I_{RMF} and RMF current phase difference ϕ. Here, ϕ represents the rotating direction of RMF, and ϕ = 90 deg. and -90 deg. denote an acceleration and deceleration phases, respectively. Moreover, we have found that $\Delta n_e/n_e$ and $\Delta v_i/v_i$ were increased in proportion to I_{RMF},[2] and they behaved nearly sinusoidal curves by changing ϕ.[13]

Here, we have further decreased f_{RMF} from 3 MHz to 1 MHz as well as 0.7 MHz with applying higher I_{RMF}, since we can easily change the rf matching conditions, e.g., series/parallel capacitances and series inductance in matching boxes in a wide range of RMF excitation frequency, and made RMF penetration condition better, at the expense of lower induced j_θ, which is proportional to f_{RMF} if a full penetration condition is satisfied. We have also investigated the dependencies of n_e and v_i on I_{RMF} and ϕ, where radial measurement positions were the same as previous experiments with f_{RMF} = 3 MHz. The present results show that the maximum $\Delta v_i/v_i$ and $\Delta n_e/n_e$ were ∼ 55 % and ∼ 360 % with f_{RMF} = 1 MHz (I_{RMF} = 46 A$_{pp}$), respectively, and these results showed that decreasing f_{RMF} with an increment of I_{RMF} can enhance the thermal thrust, which is represented as surface integrals of a static pressure $n_e\, k_B\, T_e$ and a dynamic pressure $n_i\, m_i\, v_i$,[2] where n_i is ion density (= n_e), k_B is Boltzmann constant, T_e is electron temperature, n_i is ion density, and m_i is ion mass. This is caused by higher n_e and v_i obtained by the RMF method. Moreover, radial distributions of time-varying component of RMF, $\tilde{b}_\perp$, which is orthogonal to the axial direction of the discharge tube, were measured to examine the RMF penetration condition with f_{RMF} = 0.7 MHz and 1.5 MHz by using a magnetic probe, and full and partial penetrations were consistent with expectation.[11]

This paper is organized as follows. Theoretical background of the RMF acceleration method, i.e., the process of inducing the azimuthal current j_θ, and experimental setup, including our plasma source, RMF coils, and plasma diagnostics, are described in Sec. II and III, respectively. In Sec. IV, the present RMF experimental results with f_{RMF} = 0.7 MHz and 1 MHz by changing external parameters are shown, accompanied by a better plasma performance than those with f_{RMF} = 5 MHz. Discussion, in particular, about RMF penetration condition and the thermal pressure, and conclusion of our present research is described in Sec. V and VI, respectively.

II. RMF ACCELERATION METHOD

Originally, inducing an azimuthal current j_θ by using RMF has been performed in the field of nuclear fusion, as was mentioned, and we applied this method to space plasma propulsion with higher current frequency than that of general FRC operation by one order of magnitude, considering a higher j_θ to achieve a high axial thrust effectively. Here, f_{RMF} is in the range $f_{ci} << f_{RMF} << f_{ce}$,
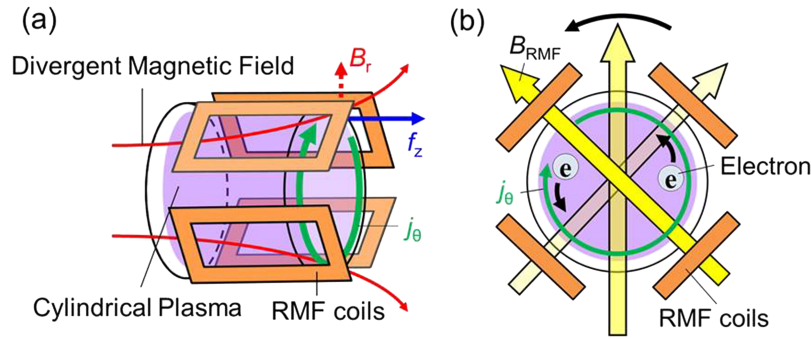
FIG. 1. Schematic diagram of the RMF coils to induce an azimuthal current j_θ, generating the axial Lorentz force f_z [(a) bird's eye view and (b) cross section view].

where f_{ci} and f_{ce} are an ion and electron cyclotron frequencies, respectively, and electrons can rotate in the azimuthal direction, as shown in Fig. 1(b). We will theoretically explain the proposed RMF acceleration process as follows. First, Rotating Magnetic Field $\mathbf{B}_{RMF}$ can be given as Eq. (1), considering a cylindrical plasma:

$$\mathbf{B}_{RMF} = B_\omega \cos\left(\omega_{RMF}\, t - \theta\right) \mathbf{e}_r + B_\omega \sin\left(\omega_{RMF}\, t - \theta\right) \mathbf{e}_\theta. \tag{1}$$

Here, ω_{RMF} is RMF current angular frequency ($= 2\pi f_{RMF}$), and B_ω is an amplitude of the rotating magnetic field, and θ is an arbitrary initial phase angle. Second, an axial oscillating electric field $\tilde{E}_z$ is induced due to the faraday's electromagnetic induction law:

$$\nabla \times \mathbf{E} = -\frac{\partial \mathbf{B}_{RMF}}{\partial t}. \tag{2}$$

Then, a time-varying axial current $\tilde{j}_z$ is induced by the Ohm's law, as shown in Eq. (3):

$$\mathbf{E} + \frac{1}{n_e e}\left(\mathbf{j} \times \mathbf{B}_{RMF}\right) = \eta \mathbf{j}. \tag{3}$$

Here, e and η are elementary charge and plasma resistivity, respectively. Third, the Hall term $<\tilde{j}_z \tilde{b}_r>$ in the second term on the LHS of Eq. (3) is proposed with the radial component $\tilde{b}_r$ [$= B_\omega \cos(\omega_{RMF}\, t - \theta)$] of $\mathbf{B}_{RMF}$. Therefore, j_θ term, which is on the RHS of Eq. (3), has a steady and a time-varying ($2\omega_{RMF}$ component) parts. Electrons can rotate in the azimuthal direction with the velocity $v_{e\theta}$, which is derived from a force balance between the drag force due to particle collisions and the driving force, and dc component of j_θ is generated as shown in Eq. (4):

$$j_\theta = -n_e e v_{e\theta}. \tag{4}$$

Finally, the axial Lorentz force f_z is generated by the product of this j_θ and an external applied radial magnetic field B_r, as shown in Eq. (5), and this schematic diagram is shown in Fig. 1(a):

$$f_z = j_\theta \times B_r. \tag{5}$$

In the full penetration condition of RMF,[8] the electrons rotate in the azimuthal direction like a rigid body rotation, and $v_{e\theta}$ can reach the maximum value $v_{e\theta\_max}$, as shown in Eq. (6):

$$v_{e\theta\_max} = r\omega_{RMF}. \tag{6}$$

III. EXPERIMENTAL SETUP

A. Large mirror device

In our experiment, we use Large Mirror Device (LMD) at Tokyo University of Agriculture and Technology, as shown in Fig. 2. The device has a 1,700-mm-long and 445-mm-inner diameter cylindrical vacuum chamber with a 1,000-mm-long quartz tube, and is evacuated by two turbo-molecular pumps, whose pumping speeds are 1,000 l/s and 2,400 l/s, respectively, with a typical back
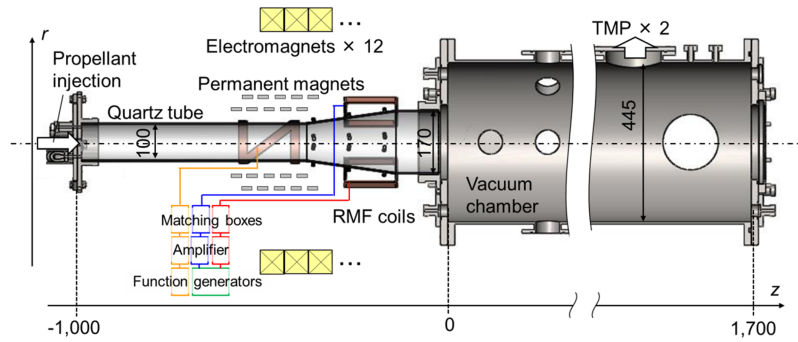
FIG. 2. Schematic diagram of LMD and peripheral apparatuses.

ground pressure of $\sim 10^{-4}$ Pa. This quartz tube has a tapered shape (100 $\sim$ 170-mm-inner diameter), expected to decrease an interaction between plasmas and the tube wall, considering a divergent magnetic field generated by permanent magnets and electromagnets. As a propellant gas, argon gas is injected continuously from a flange port located on an upstream side of the quartz tube via a mass flow controller, where the gas flow rate can be controlled up to 100 sccm. A half-helical antenna, whose azimuthal mode of $m = 1$,[16] is wound around the quartz tube to generate a plasma, whose n_e can be raised up to $\sim 10^{13}$ cm^{-3} if we use electromagnets as well as permanent magnets,[13] whose grade is N35 made by NeoMag Co. Ltd, located as shown Fig. 2. In our present experiment, only permanent magnets are used, which has non-uniform magnetic field profile, so-called magnetic nozzle.[17] This field profile makes the axial thrust through the product of the radial component of the external magnetic field B_r and the induced diamagnetic current in the azimuthal direction j_θ. In our previous experiment, the magnetic nozzle effect was investigated by the use of Laser Induced Fluorescence (LIF) method and thrust measurement by means of a target type thrust stand w/o RMF method.[18,19] An excitation rf frequency for plasma production is 7 MHz for a 75 ms pulsed discharge (5 % duty) at intervals of 1.5 s, which is controlled by a function generator. With respect to the rf discharge, a high power source (Thamway, T162-6746A), whose maximum power is $\sim$ 5 kW for the frequency with a range of 3 - 15 MHz, and used with an impedance matching box (Thamway, T020-6326AK), which can change values of parallel/series capacitances, are utilized. Here, the typical input rf power is $\sim$ 1 kW (3 kW is described only in Sec. E).

B. RMF coils

As an RMF acceleration antenna, two sets of 5 turns, opposing coils with 168-mm-axial and 115-mm-azimuthal length are at axial position of $z = -330 \sim -162$ mm in a downstream region of fr antenna, considering the divergent magnetic field shape to have the B_r component [see Eq. (5)], as shown in Fig. 2. The material of this RMF coils is oxygen-free copper, which has a 15-mm-width and a 0.5-mm-thickness, shielded by an insulation tube. Phase difference ϕ between the two-set coils' current I_{RMF} can change the rotation direction of $\mathbf{B}_{RMF}$: $\phi = 90$ and -90 degrees denote axial plasma acceleration and deceleration phases, respectively, as was mentioned. Here, I_{RMF} can be controlled by using two sets of rf power supplies (Thamway, T145-6326CK and T145-6326B), and ϕ and f_{RMF} are adjusted by a function generator, as shown in Fig. 3(a). Depending on f_{RMF} and target plasma parameters, RMF matching condition can be adjusted by using matching boxes, as shown in Fig 3(a). We apply 30 ms RMF from $t = 35$ to 65 ms for the 75 ms rf pulsed discharge. This RMF operation enables us to compare the plasma performance between the cases of w/and w/o RMF easily in one shot, and it was confirmed that the rf discharge w/o RMF does not change compared to the one after finishing RMF application ($t = 65 - 75$ ms), as shown in Fig. 3(b).

C. Plasma diagnostics

In our plasma diagnostic of local plasma flow velocity in addition to plasma density, Mach probe method has been adopted to estimate the RMF acceleration effect. A straight type Mach probe is at $z = -130$ mm to measure v_i and n_e in the downstream of RMF antenna, as shown in Fig. 4(a).
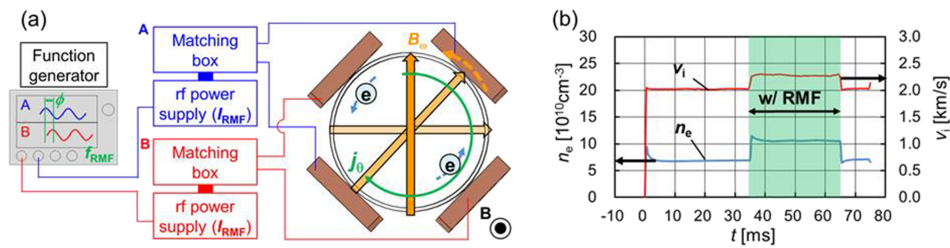
FIG. 3. Schematics of (a) RMF antenna and peripheral apparatuses and (b) example of v_i (red line) and n_e (blue line) with 30 ms RMF application (green hatched region) during 75 ms rf discharge.
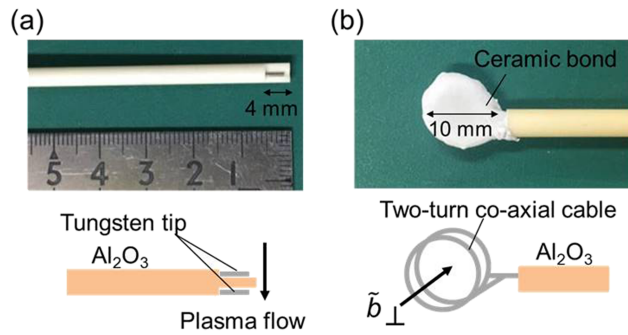

FIG. 4. Schematics of (a) a straight type Mach probe and (b) a magnetic probe.

Concerning electrodes to capture ion saturation current, two tungsten rods with a diameter of 0.8 mm are inserted into holes of an insulation Al_2O_3 tube, and an exposed length of both electrodes to a plasma is 4 mm, considering the sheath thickness.[20] The insulation tube has a separating barrier to divide a plasma flow into an upstream and a downstream sides of the electrodes. Thus, ion Mach number can be calculated by a ratio of ion saturation current densities between the two electrodes,
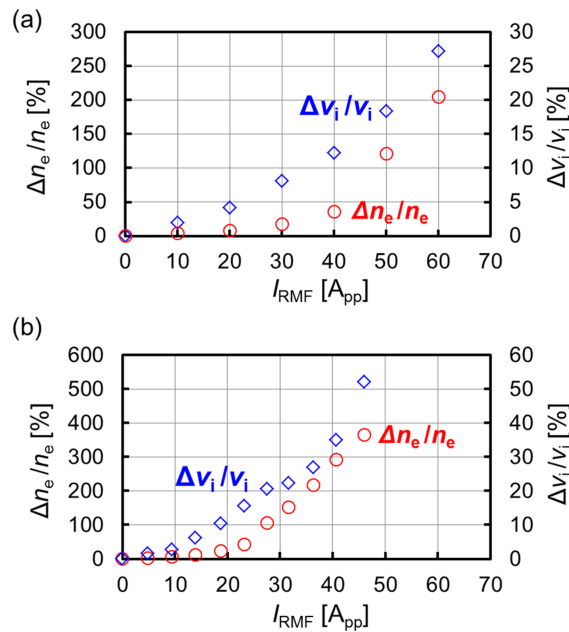

FIG. 5. Measured $\Delta n_e/n_e$ (open red circle) and $\Delta v_i/v_i$ (open blue diamond) by changing I_{RMF} at $r = 60$ mm and $z = -130$ mm with (a) $f_{RMF} = 0.7$ MHz and (b) $f_{RMF} = 1$ MHz ($P_{rf} = 1$ kW, $fr = 40$ sccm, and $\phi = 90$ deg.).

employing an unmagnetized model, whose model number κ is 1.26,[19,20] and then a local v_i can be derived, using a typical T_e of 5 eV in our experimental scheme. Generally, v_i data by a Mach probe[12] agree with the ones by Laser Induced Fluorescence (LIF) method within a factor of $\sim$ 1.5.[22] A local value of n_e can be also calculated by an average of ion saturation currents from both electrodes, and these experimental values are derived from time average of each discharge shot by shot, using eight discharges.

In addition, a measurement of time-varying component of RMF, $\tilde{b}_\perp$, which is orthogonal to the axial direction, has been conducted by using a magnetic probe, whose loop diameter and number of the turn are 10 mm and 2 turns, respectively. The probe consists of a co-axial cable inserted into insulation Al_2O_3 tube and a probe tip is coated with ceramic bond, as shown in Fig. 4(b). The coil surface, which detects the magnetic field, is vertical to the radial direction of the quartz tube, and can be scanned to obtain the radial distributions of $\tilde{b}_\perp$ at z = -250 mm, which is about the same position of the axial center of RMF coils.

IV. MEASUREMENTS RESULTS OF RMF ACCELERATION

To examine the RMF acceleration method, following experiments were performed under the experimental conditions, as shown in Table I, and experimental results presented as follows: Sec. A. $\Delta n_e/n_e$ and $\Delta v_i/v_i$ I_{RMF} with f_{RMF} = 0.7 MHz and 1 MHz, Sec. B. Radial distributions of n_e and v_i by changing fr with f_{RMF} = 0.7 MHz and 1 MHz, Sec. C. Comparisons of $\Delta n_e/n_e$ and $\Delta v_i/v_i$ between f_{RMF} = 0.7 MHz, 1 MHz, and 5 MHz, Sec. D. Dependences of $\Delta n_e/n_e$ and $\Delta v_i/v_i$ on ϕ with f_{RMF} = 0.7 MHz, and Sec. E. Radial distributions of radial component of RMF, $\tilde{b}_r$.

A. $\Delta n_e/n_e$ and $\Delta v_i/v_i$ by changing I_{RMF} with f_{RMF} = 0.7 MHz and 1 MHz

Figures 3(a) and (b) show the plots of the measured $\Delta n_e/n_e$ and $\Delta v_i/v_i$ with f_{RMF} = 0.7 MHz and 1 MHz, respectively, as a function of I_{RMF} at r = 60 mm and z = -130 mm for the case of P_{rf} = 1 kW, fr = 40 sccm, and ϕ = 90 deg. The maximum value of I_{RMF} was not same between f_{RMF} = 0.7 MHz and 1 MHz due to a different impedance matching of an rf circuit, and I_{RMF} = 0 A_{pp} means the case of without applying RMF to plasma. Here, $\Delta v_i/v_i$ as well as $\Delta n_e/n_e$ increased almost quadratically by increasing I_{RMF}. When I_{RMF} is $\sim$ 60 (46) A_{pp} with f_{RMF} = 0.7 (1) MHz, the maximum $\Delta n_e/n_e$ and $\Delta v_i/v_i$ were $\sim$ 200 (360) % and $\sim$ 27 (55) %, respectively. The increase of n_e was much higher than that of v_i in the present experimental conditions in both cases of f_{RMF}, and increasing rates of n_e and v_i were higher in the case of f_{RMF} = 1 MHz than that of f_{RMF} = 0.7 MHz at the same I_{RMF}. Therefore, a further increase of I_{RMF} with f_{RMF} = 1 MHz is expected to have the better plasma performance. These high increases of n_e contribute to the thermal thrust: dynamic pressure n_i m_i v_i^2 (the product of ion flux n_i v_i and momentum m_i v_i), and static pressure n_e k_B T_e increased by increasing I_{RMF}, which will be described in Sec. V.

B. Radial distributions of n_e and v_i by changing fr with f_{RMF} = 0.7 MHz and 1 MHz

Figures 6(a)-1 and 2 show radial distributions of n_e with f_{RMF} = 0.7 MHz (I_{RMF} = 50 A_{pp}) and 1 MHz (I_{RMF} = 30 A_{pp}), respectively, and Figs. 6(b)-1 and 2 show those of v_i, w/o and w/RMF, respectively. Here, P_{rf} = 1 kW, ϕ = 90 deg., and fr was changed: 20, 40, and 60 sccm.

TABLE I. Experimental conditions of RMF application.

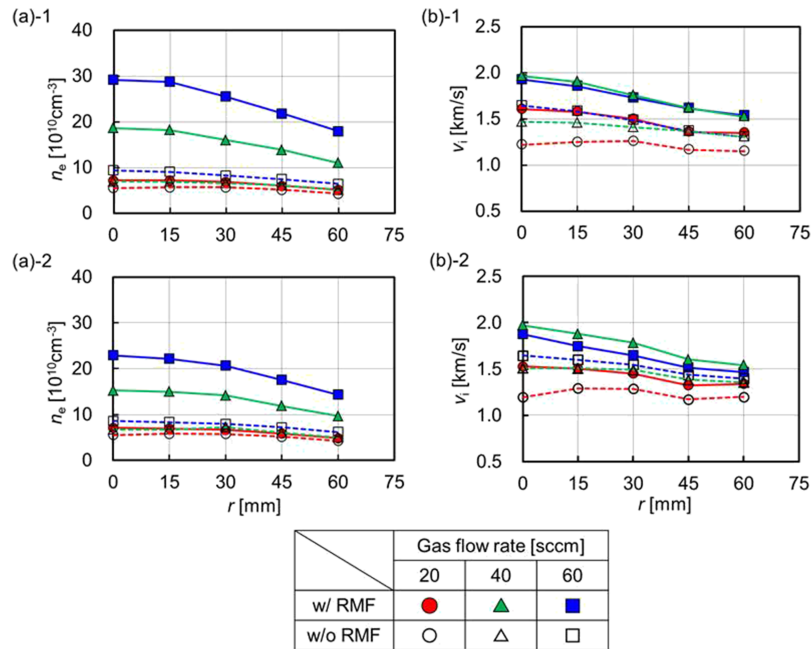| f_{RMF}	0.7 (1) MHz			
Phase difference ϕ of I_{RMF}	-180 $\sim$ 180 deg.			
RMF current I_{RMF}	$\sim$ 10 A_{pp}	$\sim$ 15 A_{pp}	$\sim$ 36 A_{pp}	$\sim$ 60 A_{pp}
Total input	$\sim$ 91 W	$\sim$ 300 W	$\sim$ 1.1 kW	$\sim$ 2.6 kW
RMF power	(~75 W)	(~165 W)	(~1.5 kW)	(-)
B_ω (center)	$\sim$ 2.0 G	$\sim$ 3.2 G	$\sim$ 6.1 G	$\sim$ 12 G
Gass flow rate fr	20, 40, 60 sccm			

FIG. 6. (a)-1 and 2 show radial distributions of n_e with f_{RMF} = 0.7 MHz and 1 MHz, respectively, and (b)-1 and 2 show those of v_i, w/(solid lines) and w/o (dotted lines) applying RMF, respectively [z = -130 mm for the case of P_{rf} = 1 kW, fr = 20 sccm (square), 40 sccm (triangle), and 60 sccm (circle), and ϕ = 90 deg.].

For both cases of f_{RMF} = 0.7 MHz and 1 MHz, n_e increased with applying RMF, and the highest values are at r = 0 mm (center of the quartz tube), and the decreases of n_e toward the outer radial direction are found in both cases of w/and w/o RMF regardless of fr. The maximum $\Delta n_e/n_e$ is ∼ 220 %, obtained at r = 15 mm for the case of fr = 60 sccm with f_{RMF} = 0.7 MHz.

With respect to v_i, it also increased with applying RMF in the entire radial positions, and the maximum value of $\Delta v_i/v_i$ was ∼ 37 %, at r = 0 mm for the case of fr = 40 sccm with f_{RMF} = 0.7 MHz. Compared to n_e, v_i did not decrease appreciably toward the outer radial direction. This maximum increment of v_i corresponds to the high $\Delta n_e/n_e$ around plasma center (pressure gradient along the z axis is also high near this region). As mentioned in Sec. A, $\Delta n_e/n_e$ and $\Delta v_i/v_i$ with f_{RMF} = 1 MHz were higher than those with f_{RMF} = 0.7 MHz with I_{RMF} = 30 A_{pp} in all radial positions.

By increasing fr, $\Delta n_e/n_e$ increased with both f_{RMF}, and the maximum $\Delta v_i/v_i$ was obtained at r = 0 mm for the case of fr = 40 sccm with both f_{RMF}. However, the maximum thermal thrust was obtained for the case of fr = 60 sccm with both f_{RMF}, since $\Delta n_e/n_e$ is higher than $\Delta v_i/v_i$ by ∼ one-order of magnitude even though the maximum $\Delta v_i/v_i$ were obtained for the case of fr = 40 sccm.

On the other hand, in terms of RMF acceleration, the degradation of an ionization rate or the collisions between an electron-ion and an electron-neutral particles by increasing fr should be considered, since these factors affect the RMF penetration and electromagnetic acceleration. In our gas pressure conditions, collision frequency between an electron-neutral particles, v_{en}, which is much larger than Coulomb collision frequency, i.e., collision frequency between electron and ion, in our experimental condition, should be calculated in order to estimate the collision effects. In this calculation, the following relations can be utilized;

$$v_{en} = 1.4 \times 10^6 T_e P_0. \tag{7}$$

Here, P_0 is neutral pressure [mTorr], and T_e is taken in unit of eV. Equation (7) comes from approximation of Brown's experimental data.[23] For typical values, v_{en} is 5.5×10^6 s^-1, assuming that neutral density does not change in the pressure of the plasma, and the electron mean free path is ∼ 17 cm for fr = 40 sccm (P_0 = 0.73 mTorr at r and z of 0 and -130 mm, respectively). Needless to say, this

collision frequency is related to resistivity η, which affects the thruster performance in this RMF method.

As discussed above, for an optimal thrust performance, we should consider these target plasma conditions, also including P_{rf} as well as RMF operation conditions. As for a thrust estimation from these radial distribution results, we will discuss this in Sec. V.

C. Comparisons of $\Delta n_e/n_e$ and $\Delta v_i/v_i$ between f_{RMF} = 0.7 MHz, 1 MHz, and 5 MHz

Figures 7(a) and (b) show radial distributions of $\Delta n_e/n_e$ and $\Delta v_i/v_i$, respectively, for the case of P_{rf} = 1 kW and fr = 40 sccm with f_{RMF} = 0.7 MHz, 1 MHz, and 5 MHz. With the decrease of f_{RMF}, $\Delta n_e/n_e$ and $\Delta v_i/v_i$ increased in the entire radial positions, although I_{RMF} = 50 A_{pp} is higher than other two cases of 30 A_{pp}. In particular, $\Delta v_i/v_i$ with f_{RMF} = 0.7 MHz and 1 MHz correspond to high $\Delta n_e/n_e$ at r = 0 mm, comparing those with f_{RMF} = 5 MHz. Decreasing f_{RMF}, increases of $\Delta n_e/n_e$ and $\Delta v_i/v_i$ were found near the plasma center, and a change of $\Delta n_e/n_e$ was higher than that of $\Delta v_i/v_i$. Nearly constant $\Delta v_i/v_i$ for the case of f_{RMF} = 5 MHz suggests a partial penetration of RMF, which will be discussed later. These decreases of f_{RMF} are better (f_{RMF} = 1 MHz may be best if I_{RMF} is same among three frequencies) compared to the case of f_{RMF} = 5 MHz with respect to plasma thrust, as was mentioned in Sec. B. Note that, as one of the important factors of these differences experimentally, the antenna-plasma coupling is also important: The RMF net power, which is absorbed by plasma, and calculated by plasma and antenna resistances, will be discussed in Sec. V.

We need to investigate experimental conditions of acceleration mechanism in addition to the electromagnetic acceleration derived from using the RMF method; e.g., the better efficiency of the axial Lorentz force, produced by diamagnetic current induced by the radial density gradient and axial force by a pressure gradient, in addition to the RMF method proposed. For future works, in order to clarify original electromagnetic acceleration, we plan to measure two-dimensional profiles of n_e and v_i to derive the density gradient in broader region of our
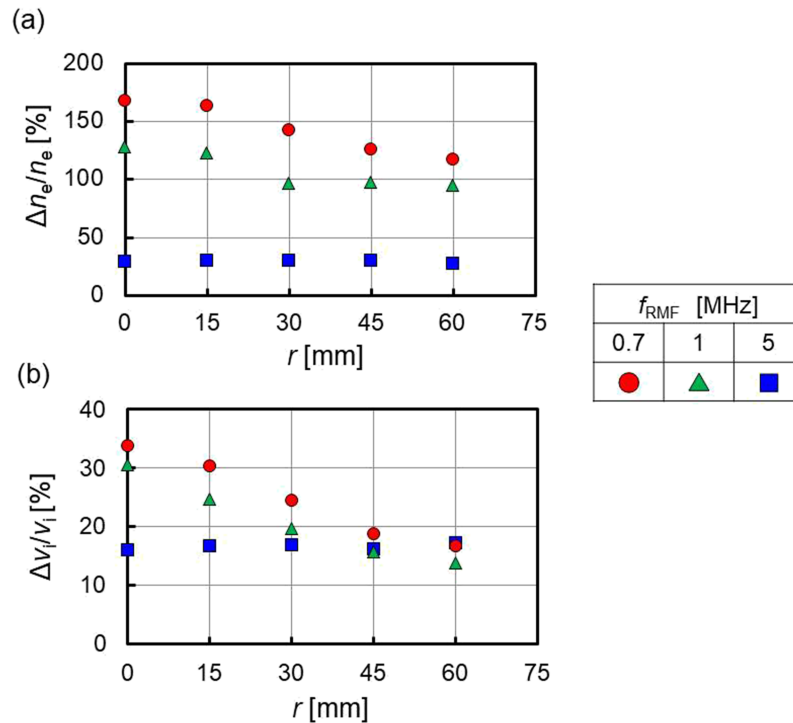

FIG. 7. Measured radial distributions of (a) $\Delta n_e/n_e$ and (b) $\Delta v_i/v_i$, comparing f_{RMF} = 0.7 MHz (I_{RMF} = 50 A_{pp}, filled circle), 1 MHz (30 A_{pp}, filled triangle), and 5 MHz (30 A_{pp}, filed square) at z = -130 mm for the case of P_{rf} = 1 kW, fr = 40 sccm, and ϕ = 90 deg.

experimental scheme. In addition, in order to distinguish the original RMF electromagnetic acceleration from that derived from diamagnetic current, as well as a measurement of time-varying $2\omega_{\mathrm{RMF}}$ component of magnetic field of RMF (or ω_{RMF} component), introducing j_θ, as will be described in Sec. V.

D. Dependences of n_e and v_i on ϕ with f_{RMF} = 0.7 MHz

Figures 8(a) and (b) show the dependences od n_e and v_i on ϕ at r = 60 mm for the case of P_{rf} = 3 kW, fr = 60 sccm, and I_{RMF} = 50 A_{pp} with f_{RMF} = 0.7 MHz. As was mentioned above, ϕ = 90 deg. and -90 deg. indicate acceleration and deceleration phases, respectively. The highest $\Delta n_e/n_e$ was ∼ 33 % for ϕ = 90 deg., and the lower was ∼ 1.7 % for ϕ = -90 deg.. Here, the nearly sinusoidal curves of n_e and v_i w/RMF was obtained as a function of ϕ, as is expected from the RMF scheme[10,13] (see Sec. II), especially, concerning v_i. The RMF coils' current might also contribute to plasma generation for this experimental condition as well as plasma acceleration, since n_e was increased with applying RMF in any phase except for ϕ ∼ -90 deg., and it is useful from a viewpoint of the thrust increment: Practically, in the case of ϕ = 90 deg., where n_e and v_i were the highest values. Here, clear wave excitation condition, such as a helicon wave to contribute to a plasma production, was not found in a previous experiment,[12] but we need to examine the dependence of plasma acceleration on ϕ in more detail, trying other experimental conditions to be checked.

E. Measurements of the orthogonal component of RMF

Measured distributions of $\tilde{b}_\perp$ with f_{RMF} = 0.7 MHz (I_{RMF} = 55 A_{pp}) and 1.5 MHz (20 A_{pp}), considering the full and partial penetration conditions od RMF, are shown in Fig.9(a) and (b), respectively. Figure 7(a) shows that the field may penetrate almost fully into a plasma, since the magnitude w/plasma is slightly higher (lower) than that w/o plasma near the plasma center (outer region). On the other hand, the tendency of partially penetration of RMF can be seen in Fig. 9(b) due to the decrease (increase) of this field in the center (outer region), compared to the case w/o RMF. Therefore, this experimental results indicate that the RMF coils can work as a RMF generation antenna to induce j_θ due to the full penetration condition. Note that we have lowered I_{RMF} to 20 A_{pp} with f_{RMF} = 1.5 MHz, in order to examine the $\tilde{b}_\perp$ distributions in partial RMF penetration condition. Here,
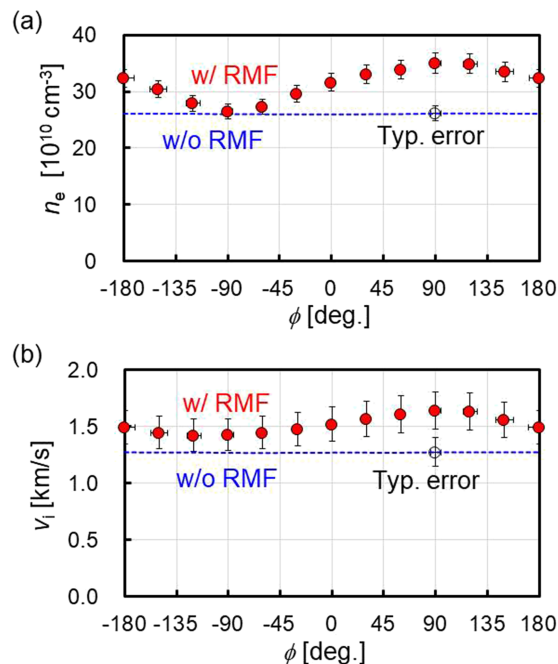

FIG. 8. Measured (a) n_e and (b) v_i by changing ϕ at r = 60 mm w/(filled circle) and w/o RMF (dotted line) for the case of P_{rf} = 3 kW, fr = 60 sccm, and I_{RMF} = 50 A_{pp} with f_{RMF} = 0.7 MHz.
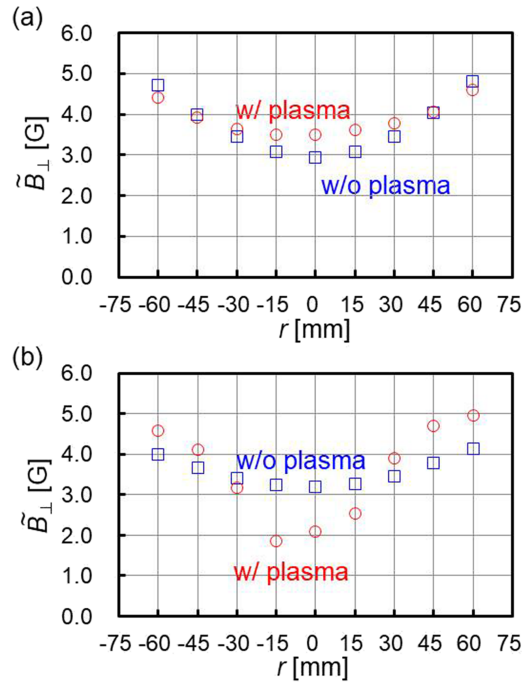
FIG. 9. Measured radial distributions of $\tilde{b}_\perp$ with (a) f_{RMF} = 0.7 MHz (I_{RMF} = 55 A_{pp}) and (b) 1.5 MHz (20 A_{pp}), which represent full and partial penetration of RMF, respectively, for the case of P_{rf} = 1 kW and fr = 40 sccm. Open circle and square symbols represent w/and w/o plasma, respectively.

the total magnetic flux may be conserved, since the field magnitude was increased (decreased) in the outer (inner) region of r > (<) 30 mm.

V. DISCUSSION

Dependencies of plasma parameters on RMF operation conditions were presented before. Moreover, both decreasing of f_{RMF} and increasing I_{RMF} under the present experimental conditions are also expected theoretically to enhance the RMF penetration condition, which is discussed in this section by using the Milroy's expression:[11]

$$\gamma_c/\lambda = \begin{cases} 1.12 & (\lambda \leq 6.5) \\ 1.12\left[1.0 + 0.12(\lambda - 6.5)^{0.4}\right] & (\lambda > 6.5). \end{cases} \tag{8}$$

Here, λ is a plasma radius normalized by a typical skin depth and γ_c is a critic value to determine RMF penetration boundary, i.e., Hall parameter: an electron cyclotron angular frequency, using the rotating magnetic field, normalized by a sum of an electron-ion and an electron-neutral collision frequencies.

The value of λ and γ can be calculated from the experimental results/conditions, and a full (partial) RMF penetration condition can be satisfied when γ/λ is larger (lower) than γ_c/λ, and these values with four f_{RMF} in the graph of Milroy's expression are shown in Fig. 8. Generally, central (edge) region shows the lower (high) value of γ/λ, leading to a worse (better) penetration condition. With f_{RMF} = 5 MHz, this field penetration condition cannot be satisfied, since λ and γ/λ are 7.5 and 0.5, respectively, at r = 0 mm in our experimental condition, as shown in Fig. 8, considering lower γ/λ value than γ_c/λ one. On the other hand, RMF could fully penetrate with only f_{RMF} = 0.7 MHz, since λ and γ/λ are 3.8 (8.2) and 1.6 (0.6), respectively, with f_{RMF} = 0.7 (1) MHz at r = 0 mm. On the other hand, λ and γ/λ are 3.0 (5.4) and 4.6 (2.2), respectively, at r = 60 mm with f_{RMF} = 0.7 (1) MHz, and γ/λ are increased with increasing r, as shown in Fig. 10. Here, in spite of a rough estimation, the full (partial) penetration condition by measuring radial distributions of RMF $\tilde{b}_r$ with f_{RMF} = 0.7 (1.5) MHz, as shown in Fig. 10, is consistent with the data in Fig. 9.
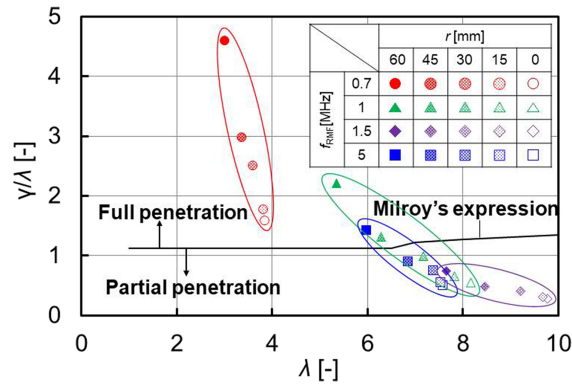
FIG. 10. Calculated γ/λ and λ with f_{RMF} = 0.7 MHz (I_{RMF} = 50 A$_{pp}$, circle), 1 MHz (46 A$_{pp}$, triangle), 1.5 MHz (20 A$_{pp}$, diamond), and 5 MHz (30 A$_{pp}$, square), in the graph of Milroy's expression. Filled symbol represents r = 60 mm and the colors become thin gradually with approaching r = 0 mm.

In order to clarify this penetration more experimentally, a measurement of RMF oscillating component by using a magnetic probe is required. In addition, from a basic point of clarifying acceleration phenomena, j_θ component of the axial Lorentz force $f_z = j_\theta \times B_r$ can be estimated by a Rogowski coil or a magnetic probe using $\nabla \times \mathbf{B} = \mu_0 \mathbf{j}$. Here, measuring $2\omega_{RMF}$ component of j_θ induced by the non-linear effects (mentioned in Sec. II), which is the same amplitude of dc component we are expecting theoretically. This can distinguish the dc component of j_θ by a radial pressure gradient from the RMF induced j_θ, as was mentioned above.

In terms of plasma acceleration, a thermal thrust F, which is represented as a sum of surface integrals of a static and a dynamic pressures, can be calculated from radial distributions of n_e and v_i, which are shown in Figs. 6(a) and (b):

$$F = \int_0^R \left(n_e m_i v_i^2 + n_e k_B T_e \right) 2\pi r \, dr. \tag{9}$$

Here, R = 85 mm is an inner radius of the quartz tube at z = -130 mm, T_e is a typical value of 5 eV, and experimental ne values are taken. By applying RMF, the plasma thrust F are calculated to be increased form ~ 1.0 mN w/o RMF to ~ 2.4 mN, ~ 5.1 mN, and ~ 1.4 mN with f_{RMF} = 0.7 MHz (I_{RMF} = 50 A$_{pp}$), 1 MHz (46 A$_{pp}$), and 5 MHz (30 A$_{pp}$), respectively. The thrust to net power ratio are changed from ~ 1.7 mN/kW w/o RMF to ~ 3.2 mN/kW, ~ 6.7 mN/kW, and ~ 1.9 mN/kW, with f_{RMF} = 0.7 MHz, 1 MHz, and 5 MHz, respectively. Here, net RF power is 580 W for P_{rf} = 1 kW, and total net RMF power were ~ 300 W, ~ 170 W, and ~ 200 W with f_{RMF} = 0.7 MHz, 1 MHz, and 5 MHz, respectively. Here, we have introduced these ratios by using the net rf and RMF powers, which is important in a physical point of view. The maximum thermal thrust is obtained with f_{RMF} = 1 MHz, but the maximum total net power was the case with f_{RMF} = 0.7 MHz, and the maximum thrust to net power ratio is in the case with f_{RMF} = 1 MHz. Based on these thrust performance, we must examine the operation parameters to achieve the better performance with f_{RMF} = 1 MHz, also considering RMF penetration condition, for a future study. The present experimental conditions were not actually optimum ones: Lower electron density, comparing to previous helicon thruster experiments w/o additional acclerations,[19] in order to demonstrate the RMF acceleration effect on plasma parameters, considering RMF penetration condition. For the purpose of increasing the thrust, in particular, with f_{RMF} = 1 MHz, the optimal experimental conditions, e.g., I_{RMF} and a number of turns of RMF coils, i.e., total ampere-turns, which increase B_{RMF}, considering optimum f_{RMF} and the inductance of RMF coils, and also a target plasma, e.g., P_{rf} and fr, should be surveyed continuously.

Theoretically, the ideal maximum axial thrust derived from the RMF electromagnetic acceleration in a full penetration condition with f_{RMF} = 0.7 MHz can be calculated roughly by Eqs. (5) and (6), and the value is ~ 40 mN with an axial length of 168 mm, which is the same as the present RMF coils' length, and radial integral region is 0 ~ 70 mm, considering the tapered shape at z = -230 mm.

This is very high from a view point of a practical electric propulsion, but the particle confinement in the external divergent, open magnetic field is poorer than that in a closed magnetic field shape like FRC, due to a short particle axial transit time. In addition, by applying electromagnets, which have not been used in present experiment, magnetic field lines do not touch the inner surface of a discharge tube,[15] and a wall loss is expected to be reduced.

VI. CONCLUSION

As an electrodeless plasma acceleration scheme, we have developed the RMF acceleration system and have carried out the experiment successfully. Here, we have utilized two pairs of 5 turns, opposed facing coils as RMF acceleration antennas with LMD, and changed RMF operation conditions including to f_{RMF}, I_{RMF}, and ϕ, in addition to target plasma conditions.

The effects of RMF current value I_{RMF} on plasma parameters, e.g., n_e and v_i, changing the current frequency f_{RMF}, have been experimentally investigated, and higher I_{RMF} leads to the higher $\Delta n_e/n_e$ as well as $\Delta v_i/v_i$: I_{RMF} contributes to plasma generation in addition to an increment of the rotating magnetic field, leading to a velocity increment [see in Figs. 5(a) and (b)]. Moreover, the maximum $\Delta v_i/v_i$ was ~ 55 % for the case of $P_{rf} = 1$ kW, $fr = 40$ sccm, $\phi = 90$ deg., and $I_{RMF} = 46$ A_{pp} with $f_{RMF} = 1$ MHz, caused partly by the higher increase of n_e [see Figs. 5(a) and (b)].

The penetration conditions could be also improved by a decrease of f_{RMF} and an increase of I_{RMF}. In a full penetration condition, axial Lorentz force f_z can be also saturated theoretically, which is in proportion to f_{RMF}. Moreover, time-varying component of RMF has been measured directly to verify the penetration condition experimentally. Therefore, the tradeoff of f_{RMF} between RMF penetration conditions and acceleration should be considered; i.e., lowering f_{RMF} is expected to improve the RMF penetration into a plasma, and on the other hand, a further increase of f_{RMF} is needed to increase the azimuthal current j_θ induced by RMF method when the RMF full penetration condition is satisfied. From the experimental results, the thermal thrusts increased with decreasing f_{RMF}, and also increasing I_{RMF}, but the absolute values have not been so high compared to the high-dense helicon experiments with electromagnets[21] due to the present experimental conditions (without these magnets), which have not been optimized.

The dependences of n_e and v_i on RMF current phase ϕ between two-facing RMF coils, in particular n_e, have been found, as a sinusoidal curve, which can be expected theoretically, and RMF coils' current could also contribute to a plasma generation. Although the deceleration and acceleration phases have been clearly demonstrated, the wave excitation mechanism, which was discussed in a previous our experiment,[12] have not been investigated this time.

In order to increase j_θ, a further increase of B_ω is expected, i.e., increases of I_{RMF} and RMF coils' turns, with an optimum coil shape, and so on, regardless the tradeoff of f_{RMF} between RMF acceleration and its field penetration. In terms of I_{RMF}, we plan to make a high-current power supply, e.g., I_{RMF} is ~ 300 A_{pp}[24] changing f_{RMF} between 0.1 - 1 MHz. Measurements of j_θ by a Rogowski coil, or time-varying component of axial magnetic field $\tilde{b}_z$ by a magnetic probe to deduce j_θ, are also helpful to estimate the axial Lorentz force and estimate the additional plasma acceleration by using RMF method.

Plasma diagnostics in addition to our present probe method, e.g., as non-contact measurements, Laser Induced Fluorescence (LIF) method,[18,22] which can measure an ion velocity and temperature without disturbing plasma, and other spectroscopies, are effective to crosscheck our previous measurement. In addition, using a thrust measurement method, e.g., a target stand type, which has a cylindrical shape, considering the collision between the target and particle[19,25] is an effective method to estimate this RMF acceleration effect.

ACKNOWLEDGMENTS

[1] D. M. Goebel, IEEE Trans. Plasma Sci. **36**, 211 (2008).

[2] V. V. Zhurin, H. R. Kaufman, and R. S. Robinson, Plasma Source Sci. Technol. **8**, R1 (1999).

[3] M. Martinez-Sanchez and J. E. Pollard, J. Propul. Power **14**, 5 (1998).

[4] F. Cannat, T. Lafleur, J. Jarrige, P. Chabert, P. -Q. Elias, and D. Packan, Phys. Plasmas **22**, 053503 (2015).

[5] F. R. Chag-Díaz, Sci. Am. **283**, 90 (2000).

[6] C. Charles, J. Phys. D: Appl. Phys. **42**, 163001 (2009).

[7] S. Shinohara, H. Nishida, T. Tanikawa, T. Hada, I. Funaki, and K. P. Shamrai, IEEE Trans. Plasma Sci. **42**, 1245 (2015).

[8] S. Shinohara, J. Plasma Fusion Res. **91**, 412 (2015) (project review paper) [In Japanese].

[9] R. W. Boswell, Phys. Lett. **33A**, 457 (1970).

[10] I. R. Jones, Phys. Plasmas **6**, 1950 (1999).

[11] R. D. Milroy, Phys. Plasmas **6**, 2771 (1999).

[12] S. Otsuka, K. Takizawa, Y. Tanida, D. Kuwahara, and S. Shinohara, Plasma Fusion Res. **10**, 3401026 (2015).

[13] T. Furukawa, K. Takizawa, D. Kuwahara, and S. Shinohara, Phys. Plasmas **24**, 043505 (2017).

[14] S. Shinohara, S. Takechi, and Y. Kawai, Jpn. J. Appl. Phys. **35**, 4503 (1996).

[15] S. Otsuka, T. Nakagawa, H. Ishii, N. Teshigahara, H. Fujitsuka, S. Waseda, T. Ishii, D. Kuwahara, and S. Shinohara, Plasma Fusion Res. **9**, 3406047 (2014).

[16] F. F. Chen, Plasma Phys. Control. Fusion **33**, 339 (1991).

[17] A. Fruchtman, K. Takahashi, C. Charles, and R. W. Boswell, Phys. Plasmas **19**, 033507 (2012).

[18] Y. Tanida, D. Kuwahara, and S. Shinohara, Trans. JSASS Aerospace Tech. Japan **14**, Pb_7 (2016).

[19] D. Kuwahara, S. Shinohara, and K. Yano, J. Propul. Power **33**, 420 (2017).

[20] M. Hudis and L. M. Lidsky, J. Appl. Phys. **41**, 5011 (1970).

[21] K. S. Chung, I. H. Hutchinson, B. Labombard, and R. W. Conn, Phys. Fluids **B1**, 2229 (1989).

[22] D. Kuwahara, Y. Tanida, M. Watanabe, N. Teshigahara, Y. Yamagata, and S. Shinohara, Plasma Fusion Res. **10**, 3401057 (2015).

[23] S. C. Brown, *Basic Data of Plasma Physics*, 2nd ed. (1967).

[24] M. Inomoto, K. Kitano, and S. Okada, Plasma Fusion Res. **3**, 004 (2008).

[25] D. Kuwahara, Y. Koyama, S. Otsuka, T. Ishii, H. Ishii, H. Fujitsuka, S. Waseda, and S. Shinohara, Plasma Fusion Res. **9**, 3406025 (2014).